Polarization of signal wave radiation generated by parametric four-wave mixing in rubidium vapor: Ultrafast (~150-fs) and nanosecond time scale excitation

C.-J. Zhu, A. A. Senin,* Z.-H. Lu,† J. Gao, Y. Xiao, and J. G. Eden
Laboratory for Optical Physics and Engineering, Department of Electrical and Computer Engineering, University of Illinois, Urbana, Illinois 61801, USA
(Received 9 November 2004; published 10 August 2005)

The polarization characteristics of the signal wave produced in Rb vapor by difference-frequency, parametric four-wave mixing (FWM) has been investigated for either ultrafast (~150 fs) or nanosecond time-scale excitation of the $5s \rightarrow \rightarrow 5d$, $7s$ two photon transitions. The electronic configurations of the $5d\,^2D_{5/2}$ and $7s\,^2S_{1/2}$ states of Rb, as well as their energy separation (~608 cm^{-1}), offers the opportunity to examine separately the resonantly enhanced $5s \rightarrow \rightarrow 7s$, $5d \rightarrow 6p \rightarrow 5s$ FWM pathways on the nanosecond time scale and then to drive both channels simultaneously with an ultrafast pulse of sufficient spectral width. As expected, dye laser (~10 ns) excitation of the $5s \rightarrow \rightarrow 5d$ ($J=5/2$) transition produces a signal wave ($\lambda_s \sim 420$ nm) having the same ellipticity as the driving optical field. Two photon excitation of Rb ($7s$) on the same time scale, however, generates an elliptically polarized signal when the pump is linearly polarized ($\varepsilon=1$), a result attributed to $7s \rightarrow 6p$, $5p$ amplified spontaneous emission at ~4 μm and ~741 nm, respectively. Simultaneous excitation of the $5s \rightarrow \rightarrow 7s$, $5d$ transitions with ~150 fs pulses centered at ~770 nm yields polarization characteristics that can be approximated as a superposition of those for the individual transitions, thus displaying weak coupling between the two FWM channels. Also, the influence of molecular contributions to the FWM signal is observed for Rb number densities above $\sim 5 \times 10^{14}$ cm^{-3}.

DOI: 10.1103/PhysRevA.72.023811 PACS number(s): 42.65.Ky, 42.65.Re, 42.50.Gy

I. INTRODUCTION

More than 30 years ago, Sorokin, Lankard, and Wynne [1,2] observed difference-frequency, parametric four-wave mixing (FWM) ($2\omega_p = \omega_s + \omega_i$, where the subscripts p, s, and i represent the pump, signal, and idler, respectively) in Cs and K and, subsequently, Hodgson *et al.* [3] reported the ability of sum-frequency FWM in Sr vapor to generate coherent radiation, tunable in the vacuum ultraviolet (vuv) spectral region. Since the initial demonstration of parametric FWM, similar experiments have been conducted with several metal vapors and gases including Na [4,5], Hg [6–8], and Kr [9], as well as H_2 [10] and NO [11]. Viewed originally as primarily a frequency conversion technique in which the idler and signal waves are capable of producing coherent emission from the vuv to the infrared, parametric FWM also has provided an invaluable diagnostic for examining a variety of coherent optical phenomena. Of particular interest is the interference of parametric FWM with incoherent or other coherent nonlinear optical processes such as amplified spontaneous emission (ASE) [12], three photon scattering [13], and stimulated hyper-Raman scattering [14]. Such competing processes exemplify a broader class of interfering quantum mechanical pathways [15] which can be applied to coherent control of chemical reaction products [16–19].

We recently demonstrated [20] that atomic wave packets can be detected optically by monitoring the signal (or idler) wave intensity generated by parametric difference-frequency FWM. Furthermore, the wave packets themselves, which behave classically as high-Q oscillators operating in the THz region, serve as sensitive detectors of molecular dissociation fragments or long range, dipole-dipole interactions [21,22]. Deriving the full benefit of this coherent optical diagnostic and, in particular, its ability to simultaneously determine the amplitude *and* phase of the interaction perturbing the wave packet, requires the FWM process to be characterized in detail.

Results are reported here for experiments in which the polarization characteristics of parametric FWM in Rb vapor have been investigated with photoexcitation on the femtosecond and nanosecond time scales. Previous experimental studies have explored the polarization characteristics of the idler or signal waves produced by FWM in Kr [9], NO [11], Hg [23], and Rb [24,25] and, in several instances [9,11], the polarization of the emitted radiation was pivotal in distinguishing FWM from another process such as amplified spontaneous emission [14]. However, all prior FWM polarization measurements have relied on pumping optical fields having durations on the nanosecond time scale. Excitation with femtosecond laser pulses provides sufficient bandwidth so as to simultaneously drive *two or more* FWM channels having the same signal frequency (or, more precisely, overlapped signal wave spectral profiles), thereby producing quantum interference in the temporal domain. The extent to which these channels are coupled is of fundamental significance and the polarization characteristics of FWM driven on the femtosecond time scale represent a previously unexplored diagnostic. The measurements described here for the $5s \rightarrow \rightarrow 7s$, $5d \rightarrow 6p \rightarrow 5s$ pathways of Rb, driven by ~150 fs pulses centered at $\lambda \sim 770$ nm, show that the degree of coupling between the two channels is low.

*Present address: VLOC, 6716 Industrial Ave., Port Richey, FL 32668, USA.
†Present address: Institute of Optics, Information and Photonics, Max-Planck Research Group, Guenther-Scharowsky-Strasse, Building 24, 91058 Erlangen, Germany.

II. THEORETICAL CONSIDERATIONS

Parametric four wave mixing is governed by the energy and momentum conservation equations:

$$2\omega_p = \omega_s + \omega_i \tag{1}$$

and

$$2\mathbf{k}_p = \mathbf{k}_s + \mathbf{k}_i \tag{2}$$

in which the subscripts p, s, and i represent parameters associated with the driving optical field (pump) and the signal and idler waves, respectively. The primary observable in the experiments reported here, the intensity of the FWM signal wave, is proportional to the square of the polarization induced in Rb vapor at the frequency ω_s by the pump field. From first-order perturbation theory, the nonlinear polarization in the direction of the pump field polarization is given by

$$\mathrm{P}_j^{(3)}(\omega_s) = \sum_{klm} \chi_{jklm}^{(3)}(-\omega_s;\omega_p,\omega_p,-\omega_i)E_{ij}^*(\omega_i)E_{pk}(\omega_p)E_{pl}(\omega_p), \tag{3}$$

where $\chi_{jklm}^{(3)}(-\omega_s;\omega_p,\omega_p,-\omega_i)$ is the tensor for the third-order nonlinear susceptibility. For an isotropic medium such as Rb vapor, only four terms of $\chi^{(3)}$ are nonzero. As a result of group symmetry, these terms are related by the expression

$$\chi_{xxxx}^{(3)} = \chi_{xxyy}^{(3)} + \chi_{yxxy}^{(3)} + \chi_{yxyx}^{(3)}. \tag{4}$$

If the pump laser and idler wave fields [$E_p(\omega_p)$ and $E_i(\omega_i)$, respectively] are both linearly polarized along the x axis, then Eq. (3) can be simplified to yield

$$\mathrm{P}_x^{(3)}(\omega_s) = \chi_x^{(3)}|\mathrm{E}_i(\omega_i)||\mathrm{E}_p(\omega_p)|^2. \tag{5}$$

Calculating the third-order nonlinear susceptibility by applying the density matrix formalism to a three (or four) level system has been described previously [25,26] and will be only briefly reviewed here [27]. For the $5s \rightarrow\rightarrow 5d \rightarrow 6p \rightarrow 5s$ FWM pathway, $\chi^{(3)}$ takes on the form [25]:

$$\chi_{jklm}^{(3)} = \sum_{abn} \frac{[\mathrm{Rb}]}{\hbar^3(\Delta_2 - \mathrm{i}\gamma_{ab})} \sum_c \frac{\mu_{ab}^j \mu_{bc}^k \mu_{cn}^l \mu_{na}^m}{(\Delta_1 - \mathrm{i}\gamma_{ac})(\omega_{nc} - \omega_p)}, \tag{6}$$

where [Rb] represents the Rb number density, $\Delta_1 = 2\omega_p - \omega_{ac}$ and $\Delta_2 = (2\omega_p - \omega_i) - \omega_{ab}$ denote the detuning of the pump frequency ω_p from the two photon resonance. The subscripts a, b, and c in Eq. (6) represent the Rb $5s, 6p$ ($J = 3/2$), and $5d$ ($J = 5/2$) states, respectively, and γ_{ac} and γ_{ab} are the relaxation rates. After summing over all odd-parity states that contribute to the two-photon transition from a to c ($5s \rightarrow\rightarrow 5d$), then the $\chi^{(3)}$ element χ_{xxxx} is given by

$$\chi_{xxxx} \equiv \chi_x^{(3)} \propto \frac{[\mathrm{Rb}]}{(\Delta_2 - \mathrm{i}\gamma_{ab})(\Delta_1 - \mathrm{i}\gamma_{ac})}. \tag{7}$$

Similarly, for the $5s \rightarrow\rightarrow 7s \rightarrow 6p \rightarrow 5s$ pathway,

$$\chi_{xxxx} \propto \frac{[\mathrm{Rb}]}{(\Delta_2 - i\gamma_{ab})(\Delta_1 - i\gamma_{ad})}, \tag{8}$$

where, in this latter case, Δ_1 is defined as $\Delta_1 = 2\omega_p - \omega_{ad}$, d denotes the $7s$ state of Rb, and γ_{ad} again represents a relaxation rate. Equations (5), (7), and (8) indicate that, for both FWM pathways, the third order nonlinear polarization is induced in the direction of the pump laser polarization. Experimental results to be described in Sec. IV, however, will show the signal wave for the $5s \rightarrow\rightarrow 7s \rightarrow 6p \rightarrow 5s$ channel to be essentially unpolarized which we attribute to the dominance of ASE.

III. EXPERIMENTAL DETAILS

The experiments reported here involve the $5s \rightarrow\rightarrow 5d$, $7s \rightarrow 6p \rightarrow 6s$ parametric FWM pathways in Rb. It has been shown [22] that these FWM processes are axially phase-matched and idler waves at ~ 5.2 and ~ 4.0 μm are generated in the vicinity of the $5d\,^2D_{5/2} \rightarrow 6p\,^2P_{3/2}$ or $7s\,^2S_{1/2} \rightarrow 6p\,^2P_{3/2}$ transitions, respectively. The signal wave, emitted at $\lambda \simeq 419.8$ nm ($\Delta\lambda \simeq 0.3$ nm FWHM for [Rb] $\sim 3 \times 10^{16}$ cm^{-3}), is associated with the $6p\,^2P_{3/2} \rightarrow 5s\,^2S_{1/2}$ transition of the atom (420.29 nm). Hartmann and colleagues [28,29] at Columbia have demonstrated that, when the $5s \rightarrow\rightarrow 5d \rightarrow 6p \rightarrow 5s$ FWM process is driven by 4 ps pump pulses, the emergence of the idler and signal is time delayed with respect to the termination of the driving optical field. Although the idler and signal are produced by superfluorescence, the two are "yoked" [28] and the entire process is coherent. As noted in the Introduction, measurements of the polarization characteristics of the signal wave reported here have been made for both nanosecond and femtosecond timescale laser excitation of the two FWM pathways. The latter offers bandwidth adequate to excite both the $5s \rightarrow\rightarrow 5d$, $7s$ two photon transitions simultaneously.

Much of the experimental apparatus and data acquisition procedures for the femtosecond studies have been described previously [21,22]. Briefly, optical pulses (~ 150 fs) having a central wavelength of ~ 770 nm, energies $\leqslant 1$ mJ, and linear polarization were generated at a repetition frequency of 1 kHz by a commercial $\mathrm{Ti:Al_2O_3}$ oscillator-regenerative amplifier system. In order to simultaneously excite the $7s$ and $5d$ states of Rb from ground, it was necessary to increase the bandwidth of the pulses exiting the amplifier and, as illustrated schematically in Fig. 1, this was accomplished by self-phase-modulation in air. Spectral broadening resulting from focusing the output of the amplifier into laboratory air with a 15 cm focal length lens was adequate to encompass both two photon $5^2S \rightarrow\rightarrow 7^2S$, 5^2D transitions. Throughout these experiments, the $\mathrm{Ti:Al_2O_3}$ oscillator/amplifier system was tuned such that the output spectrum was symmetrical and the peak wavelength corresponded roughly to the photon energy that is one-half that of the midpoint, with respect to ground, between the $7s$ and $5d$ states of Rb ($\sim 26\,010$ cm^{-1}).

After recollimation of the beam, a second lens (focal length of 25 cm) focused the optical pulses into a heat pipe or all-sapphire cell containing Rb vapor at a pressure between 2.5×10^{-3} and 20 Torr (corresponding to number den-

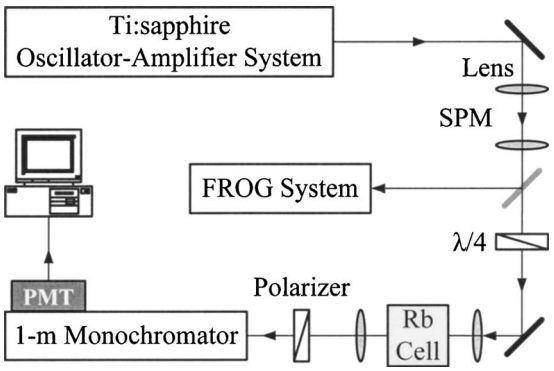

FIG. 1. Simplified schematic diagram of the experimental arrangement for studying the polarization characteristics of the signal wave generated by parametric FWM in Rb vapor with ~150 fs pulses. The acronyms SPM and PMT represent "self-phase-modulation" and "photomultiplier," respectively, and only one of the four lenses in the apparatus is identified explicitly.

sities between $\sim 6\times 10^{13}$ and 3×10^{17} cm^{-3}, respectively). The lengths of the vapor columns in the heat pipe and sapphire cell are 3–10 cm and 1.7 cm, respectively, and the sapphire cell was of particular value in carrying out experiments at the lower Rb number densities. The single pulse energy was normally kept at or below 1 μJ which produces a peak intensity in the Rb cell estimated to be $\sim 3\times 10^{10}$ W cm^{-2}.

Experiments on the nanosecond time scale were carried out with a pulsed dye laser pumped by the second harmonic of an Nd:YAG laser system producing pulses having temporal widths of nominally 8–10 ns (FWHM) and spectral linewidths of ~0.4 cm^{-1}. FWM excitation spectra were acquired by scanning the dye laser wavelength while recording the relative signal wave intensity. For both the femtosecond and nanosecond time-scale experiments, two sets of polarization measurements were made. The first entailed propagating linearly polarized pulses, produced by the Ti:Al_2O_3 amplifier (fs experiments) or dye laser, through the vapor cell and determining the polarization of the violet signal wave emerging from the vapor cell. A polarizer was rotated by a computer-controlled stage while measuring the relative intensity of the violet signal. Throughout the remainder of this paper, θ will denote the angle of rotation of the polarizer with respect to the linearly polarized pump. If the pump is elliptically polarized, θ is measured with respect to the major axis of the pump's polarization ellipse. In subsequent experiments, the ellipticity (ε) of the pump pulse (fs or ns) was controlled with a $\lambda/4$ waveplate located immediately upstream of the vapor cell. Again, the relative intensity of the generated violet signal wave was recorded.

Before leaving this section, several comments regarding processes, other than parametric FWM, excited by the driving optical field are warranted. The interference of FWM with two photon excitation of the atom and the concomitant impact on stimulated hyper-Raman scattering (SHRS) has been examined in detail for several of the alkalis over the past two decades [14,30,31]. For example, Garrett, Deng, and co-workers [14,31] have demonstrated that this interference manifests itself in a suppression of SHRS in the forward direction under weak pumping conditions. With strong excitation, however, forward-directed SHRS reemerges and its spectrum is considerably broader than that for the backward process [31].

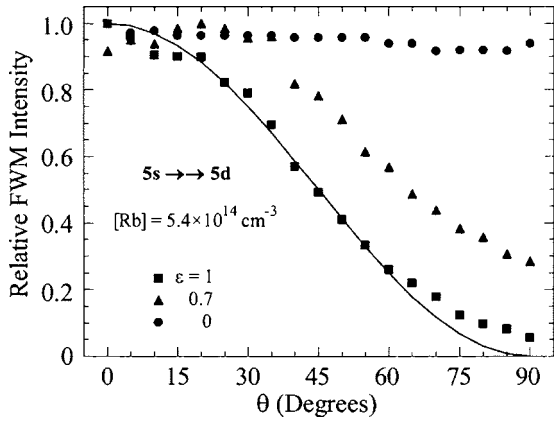

FIG. 2. Dependence of the relative FWM signal wave (~420 nm) intensity on θ, for three values of pump laser ellipticity (ε) and the dye laser tuned to the $5s\ ^2S_{1/2} \rightarrow \rightarrow 5d\ ^2D_{5/2}$ two photon transition at $\lambda \simeq 778$ nm. The Rb number density, [Rb], was 5.4×10^{14} cm^{-3} for all measurements. The solid curve represents the function $\cos^2\theta$.

The femtosecond experiments were carried out under strong pumping conditions [31] and, as will become evident in the next section, ASE competes with FWM. However, as noted in Ref. [14], "The ASE or SHR emissions can be distinguished from the parametric FWM by spectral and/or polarization differences or, in some instances, by the physical separation between conical and axial propagation, or by directionality." Indeed, the FWM processes considered here are phase-matched on axis and the ~420 nm signal wave intensity, for example, has a measured divergence of $0.9\pm 0.1°$ for $[\mathrm{Rb}]=2.9\times 10^{16}$ cm^{-3} which is in agreement with theory [20,22]. Experimentally isolating the FWM radiation is straightforward, therefore, as the 1 m monochromator of Fig. 1 was situated >1 m downstream from the Rb vapor cell. Only weak SHRS emission in the backward direction was observed, and the contribution of ASE to the detected signal can be ignored. Finally, in the experiments conducted with nanosecond time-scale pulses, the peak laser intensity was maintained at $\sim 10^5$ W cm^{-2} which is associated with weak pumping [14,31]. Consequently, the impact on these measurements of SHRS in the forward direction is negligible.

IV. RESULTS AND DISCUSSION

The results of polarization experiments in both the femtosecond and nanosecond temporal domains are described in this section. Since previous investigations of the polarization properties of the signal or idler waves in parametric FWM have dealt exclusively with ns pulse excitation, our discussion begins here as well.

A. Nanosecond time-scale data

Figure 2 illustrates the measured dependence of the rela-

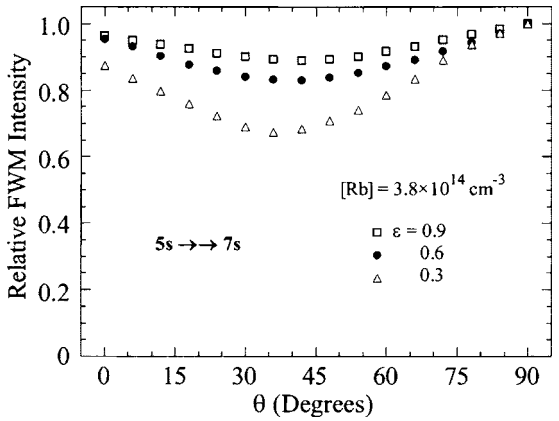

FIG. 3. Data similar to those of Fig. 2 but obtained for the input optical field tuned to the $5s\ ^2S_{1/2} \rightarrow \rightarrow 7s\ ^2S_{1/2}$ two photon transition at $\lambda \simeq 760$ nm. Results are shown for several values of ellipticity ranging from $\varepsilon = 0.3$ to 0.9 and, throughout these experiments, [Rb] was fixed at 3.8×10^{14} cm^{-3}.

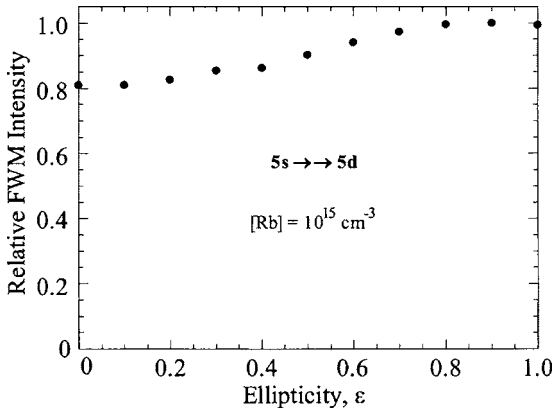

FIG. 4. Dependence of the relative signal wave (~420 nm) intensity on the ellipticity of the driving (input) optical field for the $5s \rightarrow \rightarrow 5d \rightarrow 6p \rightarrow 5s$ FWM pathway (dye laser pumped; $\lambda \simeq 778$ nm). The Rb number density was held constant at [Rb] $= 10^{15}$ cm^{-3}.

tive FWM signal wave intensity ($\lambda \sim 420$ nm) on θ when the dye laser (pump) is tuned to the $5s\ ^2S_{1/2} \rightarrow \rightarrow 5d\ ^2D_{5/2}$ two photon transition ($\lambda \simeq 778$ nm). Data are presented for several different values of the pump laser ellipticity (ε) but the Rb number density, [Rb], is fixed at 5.4×10^{14} cm^{-3}. When the dye laser beam is linearly polarized ($\varepsilon = 1$), the measurements are well described by the function $\cos^2 \theta$ (represented by the solid curve of Fig. 2) which is to be expected when the signal wave polarization follows that of the driving optical field. Consequently, as a result of momentum conservation in the parametric FWM process, the polarizations of both the driving field and the signal wave are identical and colinear for the $5s \rightarrow \rightarrow 5d \rightarrow 6p \rightarrow 5s$ FWM pathway. Similar results have been obtained by Tsukiyama [9] for Kr, Ishii *et al.*[11] for NO, and Museur *et al.* [23] for Hg. Furthermore, as ε is decreased to $\varepsilon = 0.7$ and $\varepsilon = 0$ (circular polarization), the data of Fig. 2 confirm that the signal wave polarization continues to follow that of the input field.

Behavior contrasting with that of Fig. 2 is observed if the pump is tuned to the two photon $5s\ ^2S_{1/2} \rightarrow \rightarrow 7s\ ^2S_{1/2}$ transition at $\lambda \simeq 760$ nm. As shown in Fig. 3 for [Rb] $= 3.8 \times 10^{14}$ cm^{-3}, the data exhibit little sensitivity to θ when $\varepsilon = 1$ (linear polarization), indicating that the $6p \rightarrow 5s$ signal wave is largely unpolarized. This result is quite similar to the polarization characteristics of the idler wave at 758.9 nm, produced in Kr by the $4p^6\ ^1S_0 \rightarrow \rightarrow 5p[1/2]_0 \rightarrow 5s[3/2]_1 \rightarrow {}^1S_0$ process, reported by Tsukiyama [9]. Ishii *et al.* [11] have observed analogous behavior in NO when specific rotational states of $C\ ^2\Pi_{1/2,3/2}(v' = 0)$ are excited from ground ($X\ ^2\Pi_{1/2,3/2}$) by two photon absorption. Amplified spontaneous emission generated on $C\ ^2\Pi \rightarrow A\ ^2\Sigma$ transitions of the molecule couples with the driving optical field to produce by FWM an unpolarized ultraviolet signal wave, confirming that the overall mixing process is not purely parametric. We conclude that two photon excitation of the Rb ($7s$) state from ground on the ~10 ns time scale and $\varepsilon \approx 1$ generates ASE on the $7s \rightarrow 6p$ transitions which culminates in an unpolarized signal at 420 nm and, therefore, the essentially featureless characteristics of Fig. 3. The conclusion that ASE plays a greater role in the $5s \rightarrow \rightarrow 7s$ measurements of Fig. 3 than is observed when the $5s \rightarrow \rightarrow 5d$ channel is excited (Fig. 2) is not surprising. Two photon excitation of the $5d$ ($J = 5/2$) state of Rb is resonantly enhanced by the $5p$ ($J = 3/2$) level and the detuning from resonance ($\hbar\omega - E_{5p}$) is ~35 cm^{-1}. For the $5s \rightarrow \rightarrow 7s$ process, however, the detuning rises by almost an order of magnitude, thereby reducing the susceptibility for the FWM process [12] and weakening the parametric process relative to competing mechanisms such as ASE, despite the suppression of SHRS owing to the low pumping intensity. Note also that, for the smaller values of pump ellipticity ($\varepsilon = 0.1, 0.4$), the data of Fig. 3 exhibit a pronounced decrease in FWM intensity in the vicinity of $\theta = \pi/4$.

When the ellipticity of the driving (dye laser) optical field is varied and one now records the relative signal wave intensity, the data of Figs. 4 and 5 are obtained. As one might expect, if the $5s \rightarrow \rightarrow 5d$ ($J = 5/2$) FWM pathway is pumped by the dye laser tuned to ~778 nm (cf. Fig. 4), only a slight

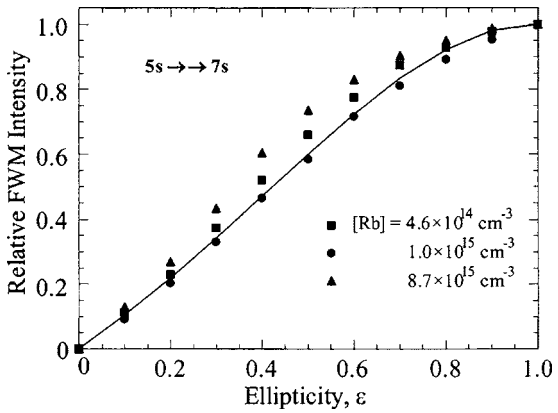

FIG. 5. Variation of the relative FWM signal wave intensity with the ellipticity ($0 \leq \varepsilon \leq 1$) of the ~8 ns pump laser beam, tuned to $\lambda \simeq 760$ nm ($5s \rightarrow \rightarrow 7s$ pathway). Results are shown for three values of Rb number density and the solid curve represents the function $\cos^2 \theta - \sin^2 \theta$, where θ and ellipticity are related by $\varepsilon = 1 - \tan \theta$.

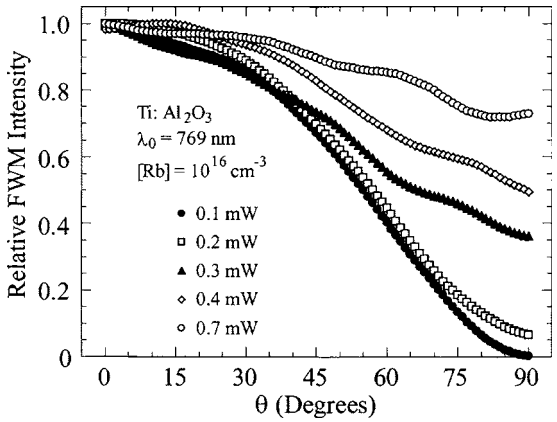

FIG. 6. Variation of the 420 nm (signal wave) intensity with θ for linearly polarized, ~150 fs pulses incident on Rb vapor at a number density of $[\mathrm{Rb}]=10^{16}$ cm^{-3}. The laser spectrum is centered at 769 nm and data are shown for several values of average laser power for which the pulse repetition frequency (PRF) is 1 kHz.

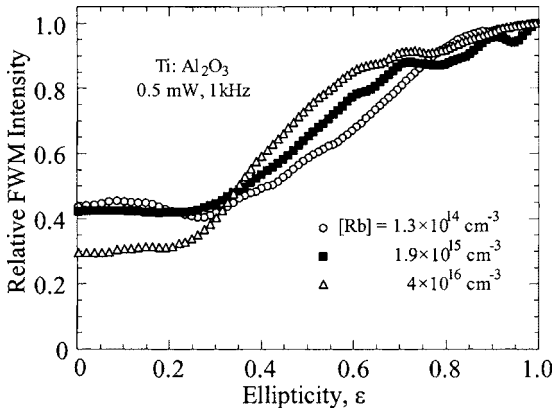

FIG. 7. Data similar to those of Figs. 4 and 5 but for ~150 fs pulses from a $\mathrm{Ti:Al_2O_3}$ laser system. The dependence of violet signal intensity on ε is given for three values of Rb number density. The average power and PRF of the laser are 0.5 mW and 1 kHz, respectively.

variation in the violet signal intensity is observed as ε is increased from zero to one. Selection rules [32] for two photon absorption permit optical excitation of this transition ($\Delta J=+2$) with either linear or circular polarization. Accordingly, the signal wave polarization of Fig. 4 follows that of the input field, as discussed earlier. Figure 5 illustrates the measured dependence of the relative FWM signal wave intensity on ε for the $5s\rightarrow\rightarrow 7s$ FWM pathway (dye laser $\lambda \simeq 760$ nm). Data obtained at lower Rb number densities ($[\mathrm{Rb}]\lesssim 5\times10^{14}$ cm^{-3}) follow quite closely the solid curve of Fig. 5 which represents the function $f(\theta)=\cos^2\theta-\sin^2\theta$, where ellipticity is related to θ by the expression: $\varepsilon=1-\tan\theta$. Since the $5s\rightarrow\rightarrow 7s$ ($\Delta J=0$) transition is forbidden for circular polarization [32], the FWM intensity in Fig. 5 is zero for $\varepsilon=0$, but rises as the ellipticity is gradually changed to $\varepsilon=1$ (linear polarization).

The behavior of the data of Fig. 5 at higher Rb densities is also of interest. It is clear that, for $[\mathrm{Rb}]\gtrsim 5\times10^{14}$ cm^{-3}, the data deviate significantly from expected behavior (represented by the solid curve). The discrepancy is particularly evident in the $0.3\lesssim\varepsilon\lesssim 0.6$ interval, where the signal wave intensity increases by as much as ~30% when [Rb] is raised by roughly an order of magnitude above 5×10^{14} cm^{-3}. This result is attributed to the rapidly rising influence of Rb dimers at the higher [Rb] values [33]. At $[\mathrm{Rb}]=5\times10^{14}$ cm^{-3}, for example, the $\mathrm{Rb_2}$ number density is $\sim 1.2\times10^{12}$ cm^{-3}, but when [Rb] is increased to 9×10^{15} cm^{-3}, $[\mathrm{Rb_2}]$ has risen to $\sim 5.8\times10^{13}$ cm^{-3}, which corresponds to ~0.65% of the monomer number density. The conclusion that Rb dimers contribute significantly to FWM in this temperature range is borne out by laser excitation spectroscopic experiments in which the ~420 nm FWM intensity is monitored as the dye laser wavelength is scanned. Although the details of these spectra will be discussed elsewhere, suffice it to say that molecular structure is prevalent in the 760–778 nm region, which serves as a reminder that the molecular contribution to the polarization behavior of FWM in Rb cannot be ignored when interpreting data acquired for $[\mathrm{Rb}]\gtrsim 5\times10^{14}$ cm^{-3} ($[\mathrm{Rb_2}]\gtrsim 10^{12}$ cm^{-3}).

B. Femtosecond excitation

With the experimental arrangement of Fig. 1, measurements similar to those discussed in the last section, but on the ~150 fs time scale, were made. In this instance, however, the bandwidth afforded by the $\mathrm{Ti:Al_2O_3}$ mode-locked system allows for *both* FWM pathways ($5s\rightarrow\rightarrow 7s, 5d\rightarrow 6p\rightarrow 5s$) to be driven simultaneously. It has been shown previously [20] that doing so produces a wave packet comprising the $7s$ and $5d$ states, and that the temporal behavior of the wave packet can be monitored by recording the relative intensity of the idler or signal waves produced by a pair of identical pump pulses separated in time by Δt. The theoretical formalism describing the coupling of the wave packet to the FWM process has been treated in detail in Ref. [22] and will not be discussed further here.

Figure 6 summarizes the results of measurements of the polarization of the signal wave produced by linearly polarized fs optical pulses for several values of the single pulse energy. These data, representative of those from 15 sets of experiments, were obtained as a function of θ for the Rb number density fixed at $[\mathrm{Rb}]=10^{16}$ cm^{-3} and the average laser power varied from 0.1 to 0.7 mW (pulse repetition frequency of 1 kHz). At the lower power levels, the results are remarkably similar to those of Fig. 2 in which the FWM process proceeded solely through the $5s\rightarrow\rightarrow 5d\rightarrow 6p\rightarrow 5s$ channel. That is, the polarization of the signal wave mimics that of the pump—both are linearly polarized and their polarizations are colinear. As discussed earlier (Sec. IV A), the dominance of the $5d$ channel at (relatively) low pump intensities is attributable to enhancement of the $5s\rightarrow\rightarrow 5d$ two photon process by the single photon near-resonance (detuning ~35 cm^{-1}) with the $5p\,(J=3/2)$ state. As the single pulse energy is increased from 100 nJ ($P_{\mathrm{av}}=0.1$ mW) to 700 nJ, however, the signal wave gradually becomes depolarized which appears to be the result of the rapid increase in the two photon $5s\rightarrow\rightarrow 7s$, $5d$ excitation rate, and the associated growing influence of ASE, as the peak intensity of the driving optical field is increased.

Consider now the dependence of the signal wave intensity on the pump ellipticity. Results are presented in Fig. 7 for three values of [Rb] ranging from 1.3×10^{14} to 4×10^{16} cm^{-3} and the laser average power held constant at 0.5 mW. A comparison of the femtosecond data of Fig. 7 with the longer pump pulse measurements presented earlier shows that the former can be represented as the weighted sum of Figs. 4 and 5. For $\varepsilon\lesssim0.25-0.3$, for example, the signal intensity of Fig. 7 is flat but rises approximately linearly for $0.3\leqslant\varepsilon\leqslant1.0$. In retrospect, this is precisely what one might have expected *if the coupling between the* 7*s and* 5*d FWM channels can be neglected*—namely, the simultaneous excitation of both the $5s\rightarrow\rightarrow7s$, $5d$ pathways with fs pulses would yield polarization behavior resembling the sum of that for the two channels photoexcited separately. Of course, this result is contingent upon adjusting the $Ti:Al_2O_3$ laser/amplifier spectrum as described in Sec. III (i.e., such that the two photon pump spectrum overlaps the $5s\rightarrow\rightarrow5d$ and $5s\rightarrow\rightarrow7s$ transitions symmetrically) but these results suggest that similar polarization measurements in other FWM systems with femtosecond time scale pulses might serve as a tool to investigate coupling between competing parametric channels. Finally, as was the case for nanosecond excitation (Fig. 5), the influence of Rb_2 dimers is increasingly apparent as [Rb] rises.

V. SUMMARY

Experiments have been described in which the polarization characteristics of the signal wave generated in Rb vapor by FWM with either fs or ns pulse excitation have been studied. Driving the two photon $5s\rightarrow\rightarrow5d$ ($J=5/2$) transition with dye laser radiation ($\sim$8 ns pulses) yields a signal wave at 420 nm whose polarization characteristics closely follow those of the input optical field. The observed behavior of the signal wave is quite different, however, if the $5s\rightarrow\rightarrow7s$ pathway is selectively excited. A linearly polarized driving optical field generates an elliptically polarized signal wave which indicates the influence of ASE. When both FWM pathways are excited simultaneously with broadband fs pulses, the behavior of the signal wave polarization can be approximated as the sum of the two individual channels. ASE is, again, an important factor as the laser pulse energy is increased and Rb dimers noticeably influence the polarization characteristics of the signal wave, irrespective of the excitation pulse width, for Rb number densities above $\sim5\times10^{14}$ cm^{-3} ($[Rb_2]\gtrsim10^{12}$ cm^{-3}). Although of fundamental interest in confirming theoretical predictions and offering an experimental vehicle by which coupling between competing FWM channels can be explored, the results reported here are also expected to be of value whenever FWM serves as a diagnostic in monitoring atomic or molecular wave packets.

ACKNOWLEDGMENT

The technical assistance of K. Collier and the support of this work by the U.S. Air Force Office of Scientific Research under Grants F49620-00-1-0372 and F49620-03-1-0391 are gratefully acknowledged.

[1] P. P. Sorokin and J. R. Lankard, IEEE J. Quantum Electron. **9**, 227 (1973).
[2] P. P. Sorokin, J. J. Wynne, and J. R. Lankard, Appl. Phys. Lett. **22**, 342 (1973).
[3] R. T. Hodgson, P. P. Sorokin, and J. J. Wynne, Phys. Rev. Lett. **32**, 343 (1974).
[4] W. Harting, Appl. Phys. **15**, 427 (1978).
[5] R. K. Wunderlich, W. R. Garrett, R. C. Hart, M. A. Moore, and M. G. Payne, Phys. Rev. A **41**, 6345 (1990).
[6] F. S. Tomkins and R. Mahon, Opt. Lett. **6**, 179 (1981); R. Mahon and F. S. Tomkins, IEEE J. Quantum Electron. **QE-18**, 913 (1982).
[7] J. Bokor, R. R. Freeman, R. L. Panock, and J. C. White, Opt. Lett. **6**, 182 (1981).
[8] R. Hilbig and R. Wallenstein, IEEE J. Quantum Electron. **QE-19**, 1759 (1983).
[9] K. Tsukiyama, J. Phys. B **29**, L345 (1996).
[10] U. Czametzki and H. F. Döbele, Phys. Rev. A **44**, 7530 (1991).
[11] J. Ishii, Y. Ogi, Y. Tanaka, and K. Tsukiyama, Opt. Commun. **132**, 316 (1996).
[12] M. S. Malcuit, D. J. Gauthier, and R. W. Boyd, Phys. Rev. Lett. **55**, 1086 (1985).
[13] Y. Shevy, S. Hochman, and M. Rosenbluh, Opt. Lett. **13**, 215 (1988).
[14] W. R. Garrett, M. A. Moore, R. C. Hart, M. G. Payne, and R. Wunderlich, Phys. Rev. A **45**, 6687 (1992).
[15] P. B. Chapple, K. G. H. Baldwin, and H.-A. Bachor, J. Opt. Soc. Am. B **6**, 180 (1989).
[16] M. Shapiro, J. W. Hepburn, and P. Brumer, Chem. Phys. Lett. **149**, 451 (1988).
[17] P. Brumer and M. Shapiro, Acc. Chem. Res. **22**, 407 (1989).
[18] See, for example, W. R. Garrett and Y. Zhu, J. Chem. Phys. **106**, 2045 (1997).
[19] C. Chen, Y.-Y. Yin, and D. S. Elliott, Phys. Rev. Lett. **64**, 507 (1990).
[20] H. C. Tran, P. C. John, J. Gao, and J. G. Eden, Opt. Lett. **23**, 70 (1998).
[21] A. A. Senin, H. C. Tran, J. Gao, Z. H. Lu, C. J. Zhu, A. L. Oldenburg, J. R. Allen, and J. G. Eden, Chem. Phys. Lett. **381**, 53 (2003).
[22] Z. H. Lu, C. J. Zhu, A. A. Senin, J. R. Allen, J. Gao, and J. G. Eden, IEEE J. Sel. Top. Quantum Electron. **10**, 159 (2004).
[23] L. Museur, C. Olivero, D. Riedel, and M. C. Castex, Appl. Phys. B: Lasers Opt. **70**, 499 (2000).
[24] S. S. Vianna, P. Nussenzveig, W. C. Magno, and J. W. R. Tabosa, Phys. Rev. A **58**, 3000 (1998).
[25] W. C. Magno, R. B. Prandini, P. Nussenzveig, and S. S. Vianna, Phys. Rev. A **63**, 063406 (2001).
[26] Y. R. Shen, *Principles of Nonlinear Optics* (Wiley, New York, 1980).
[27] A more rigorous treatment of the problem will account for the sublevel structure of the relevant atomic states but the development summarized here is adequate for interpreting the experiments.

[28] J. H. Brownell, X. Lu, and S. R. Hartmann, Phys. Rev. Lett. **75**, 3265 (1995).

[29] A. I. Lvovsky, S. R. Hartmann, and F. Moshary, Phys. Rev. Lett. **82**, 4420 (1999).

[30] See, for example, D. Cotter, D. C. Hanna, W. H. W. Tuttlebee, and M. A. Yuratich, Opt. Commun. **22**, 190 (1977).

[31] L. Deng, W. R. Garrett, M. G. Payne, and D. Z. Lee, Opt. Commun. **142**, 253 (1997).

[32] K. D. Bonin and T. J. McIlrath, J. Opt. Soc. Am. B **1**, 52 (1984).

[33] M. Lapp and L. P. Harris, J. Quant. Spectrosc. Radiat. Transf. **6**, 169 (1966).